Solar RRL
www.solar-rrl.com

Natural Product Additive with Multifunctional Groups Enhancing the Efficiency and Stability of Perovskite Solar Cells

Yonglei Han, Chao Zhou, Shuchen Weng, Guicheng Yu, Fang Lin, Hanlin Hu, Yongfei Wang, and Haoran Lin**

Perovskite solar cells (PSCs) are widely studied as the most promising photovoltaic technology, but their performance is sensitive to the morphology and the defect density of the perovskite films. Herein, additive engineering strategy is applied to further improve the film morphology and device performance by doping a small amount of natural product, D-Aspartic acid (D-2-Aminobutanedioic acid, D-Asp), into perovskite precursor solution. The modified device exhibits a greatly enhanced power conversion efficiency of 22.7%, which is unprecedented for PSCs doped with natural amino acids, and 3000 h stability in ambient air is achieved. Through systematical characterizations, it is concluded that D-Asp could result in thicker film formation, outstanding perovskite film morphology, and reduced defect sites passivated by the multiple functional groups. The results prove that the performance and stability of the state-of-the-art mixed ion PSCs with regular architecture could be effectively enhanced by D-Asp. The minimum usage of the natural product as an additive is beneficial for the fabrication process and cost-control in the industrialization of PSCs. This work also highlights the different passivating mechanisms for the molecules with multiple functional groups which are meaningful for materials design.

1. Introduction

The global environment is constantly affected by the consumption of fossil fuels and the emission of greenhouse gases. Exploring new renewable energy sources for carbon neutrality has become an inevitable goal, and the solar cells that harvest solar energy without any emissions have become the current research hotspot.[1]

Metal halide perovskite solar cells (PSCs) are a prosperous developing technology that could likely compete with silicon solar cells in the future. Benefitting from the excellent properties of metal halide perovskite materials such as suitable bandgap, high light absorption coefficient, high charge carrier mobility, and high defect tolerance, the power conversion efficiencies (PCEs) of PSCs have increased from 3.8% to 25.7% in the past decades,[2,3] achieving about 80% of the Shockley–Quisser (SQ) limit.[4] Although their PCEs have reached a considerable level for industrialization, the state-of-the-art PSCs still suffer from ambient instability, ion migration, and interfacial reactions, which deteriorate their performance under working conditions.

Tremendous research have shown that defects in metal halide perovskites could generate trap states within the bandgap, and the charges captured by deep traps will irreversibly go through nonradiative recombination, harming the open-circuit voltage (V_{OC}), short-circuit current (J_{SC}), and fill factor (FF) simultaneously.[5] In contrast, defect sites are more vulnerable to moisture, oxygen, light, and heat, which significantly reduce the lifetime of the device.[6–8] In addition, the ion migration in perovskite material under an electric field would cause phase separation, hysteresis, and interfacial reaction, which would also be exacerbated by the increase of defect density.[9]

To alleviate the negative influences introduced by the defects, multiple defect passivation methods were proposed such as transport layer passivation,[10–12] surface treatment,[13–16] and additive engineering.[17–19] Additive engineering is the most facile and cost-effective method in which a small amount of elaborately chosen additives are premixed in the precursor solution of perovskite, effectively passivating the defects on the surface, grain boundaries, and in the bulk when the perovskite film is formed.

Organic additives were widely used for defect passivation due to their structural versatility and ability to passivate different types of defects.[20] For example, the ammonium salts are capable of passivating the A site (refer to the small cation site of the metal halide perovskite such as Cs^+, $CH_3NH_3^+$) vacancy on the perovskite surface by forming hydrogen bonds with halide atoms,

Y. Han, C. Zhou, Y. Wang
School of Materials and Metallurgy
University of Science and Technology Liaoning
Anshan 114051, China
E-mail: wyf8307@ustl.edu.cn

Y. Han, C. Zhou, S. Weng, G. Yu, F. Lin, H. Hu, H. Lin
Hoffmann Institute of Advanced Materials
Shenzhen Polytechnic
Shenzhen 518055, China
E-mail: hlin@szpt.edu.cn

The ORCID identification number(s) for the author(s) of this article can be found under https://doi.org/10.1002/solr.202200998.

DOI: 10.1002/solr.202200998

making them the most commonly used organic additive for PSCs. Feng et al. employed different unilateral alkylamine additives with different chain lengths and found that the open-circuit voltage (V_{OC}) and FF of PSCs were both improved.[21] Wu et al. added different bilateral alkylamine additives in the perovskite precursor solution, which passivated two A site vacancies with the ammonium groups at both ends to expose the hydrophobic alkyl chain outside and increased the moisture resistance of the perovskite films.[22] Carboxylic acids, as Lewis-base organic additives, could passivate the X site (X stands for halide) vacancy by forming a coordination bond with the under-coordinated Pb atoms. Wu et al. adjusted the electron-donating ability of the carboxyl group by manipulating the functional groups on the organic molecule, and successfully enhanced the interaction between the additive and exposed Pb atoms on the perovskite.[23] Li et al. employed a large molecular organic dye (AQ310) as an additive, in which the passivation effect of –COOH was evidenced by time-of-flight secondary-ion mass spectrometry (TOF-SIMS) and Fourier transform infrared spectroscopy (FTIR).[24]

Organic additives with multiple functional groups could passivate multiple types of defects in perovskite with a minimum doping ratio, which is advantageous for the cost-control of practical PSCs. For example, Yun et al. used the rigid p-aminobenzoic acid iodide (PABA·HI) to passivate the grain boundaries in perovskite films, and the device maintained over 91% of the initial efficiency after exposure to 75% humidity for 312 h.[25] Lin et al. studied flexible amino acids with different chain lengths and found that the effect of amino acid chain length on the stability of PSCs devices can be ignored.[26]

Easily available natural amino acids are perfect choices for the defect passivation of perovskite. For example, Kim et al. fabricated inverted PSCs with L-alanine as an additive which formed inner salt in a proper pH condition, and increased PCE from 18.3% to 20.3% was obtained for small area devices.[27] Hu et al. added four natural amino acids, glycine, glutamic acid, proline, and arginine separately to the perovskite precursor solutions, and deeply studied the passivation mechanism of arginine on the perovskite film.[28] Other than that, a couple of other natural amino acids have been used as additives in PSCs and achieved enhanced device performance.[27,29–31] However, the previously reported PCEs for the PSCs with natural amino acid additives are relatively low (less than 21%), which is probably due to the usage of simple composition perovskite $MAPbI_3$ (Table S1, Supporting Information). In addition, the PCE enhancement of the devices based on regular architecture (n-i-p) upon doping are usually as low as ≈5% except in one case a PCE enhancement of 10.1% was achieved upon proline doping.[30] Since mixed ion PSCs with regular architecture have allowed record efficiencies,[32] the influence of natural amino acids on this type of PSCs needs further investigation.

Here, we report a natural product, D-Aspartic acid (D-2-Aminobutanedioic acid, Figure S1, Supporting Information, simplified as D-Asp), with one amino group and two carboxyl groups on the molecule as an additive for PSCs with mixed ion composition ($MA_{0.27}FA_{0.73}PbI_{2.64}Br_{0.06}Cl_{0.3}$). The PSC device with regular (n-i-p) architecture doped with 0.3 wt% of D-Asp exhibited a champion PCE of 22.7%, which is 10.2% higher than that of the undoped device. The PCE is higher than that of all previously reported PSCs doped with natural amino acids, suggesting the performance of PSCs based on mixed ion compositions could also be effectively enhanced by natural amino acids. The 10.2% PCE enhancement is also the highest compared with that of the regular devices in Table S1, Supporting Information, highlighting the uniqueness of D-Asp. The efficiency of the unencapsulated device remained almost unchanged after 2000 h storage in a nitrogen atmosphere, while maintaining 93% of the initial efficiency after 3000 h storage in ambient condition. Through systematical characterizations, we observed thicker film formation upon D-Asp doping, while having improved film morphology with fewer surface defects and higher crystallinity. The enhanced device performance was also attributed to the outstanding defect passivation effect of D-Asp, which significantly reduced defect density and undesired non-radiative recombination. Our work proves that organic additives with multiple functional groups are promising in achieving highly efficient and stable PSCs with a small doping ratio.

2. Results and Discussion

To determine the best doping ratio of the D-Asp additive, we characterized and compared the film morphology of the pristine perovskite with the composition of $MA_{0.27}FA_{0.73}PbI_{2.64}Br_{0.06}Cl_{0.3}$ and the perovskite doped with different ratios of D-Asp (from 0.1% to 3%). The perovskite films were prepared by a one-step spin-coating method and analyzed after annealing. The top-view scanning electron microscope (SEM) images of the perovskite films displayed in **Figure 1** clearly show that there are significant pinhole defects between the grains of perovskite polycrystals doped with 0, 0.1, 0.5, 1, 3 wt% of D-Asp (Figure 1a,b,d–f). In contrast, for the perovskite film doped with 0.3 wt% of D-Asp, the grains are tightly packed without obvious pinhole defects (Figure 1c). When large doping ratios are applied (1 and 3 wt% of D-Asp, Figure 1e,f), a new amorphous phase covering part of the perovskite surface is observed, which is believed to be the D-Asp reprecipitation due to its low solubility. The insulating organic phase formed on the surface of the perovskite film could inhibit interfacial charge transfer between the perovskite and charge transporting layer. Therefore, we preliminarily consider that 0.3 wt% could be the best doping ratio for PSCs.

Another observable influence of the D-Asp additive on the perovskite films is better crystallinity.[33] Figure S2, Supporting Information, shows that the statistic grain size of the perovskite films increases from 790 to 1060 nm when the doping ratio of D-Asp increases from 0% to 3%. This suggests that increasing the D-Asp amount could improve the crystallinity of perovskite polycrystals. The energy-dispersive spectroscopy (EDS) mapping of the perovskite film with 0.3 wt% as shown in Figure S3, Supporting Information, suggests the homogeneous distribution of Pb, I, C, N, O elements.

The good crystallinity of the doped perovskite films was also demonstrated by the X-ray diffraction (XRD) characterization. As shown in **Figure 2**, the XRD patterns of the doped films are very similar to that of the pristine film which suggests the addition of the D-Asp did not alter the crystal structure or crystal orientation significantly.[34] We magnified the characteristic (110) diffraction peaks of the perovskite films and observed that the peaks of the doped films have slightly reduced full width at half maximum

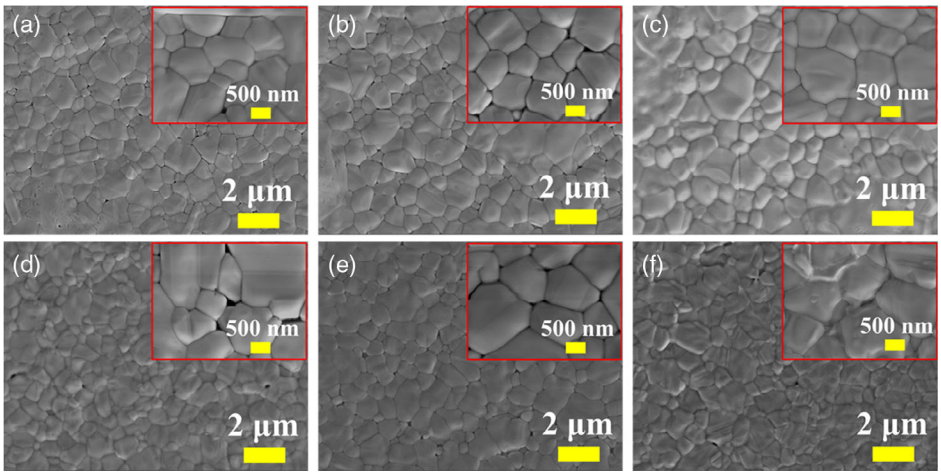

Figure 1. Top-view scanning electron microscope (SEM) images of pristine perovskite and D-Asp-doped perovskites with different doping ratios of: a) 0 wt%, b) 0.1 wt%, c) 0.3 wt%, d) 0.5 wt%, e) 1 wt%, and f) 3 wt%.

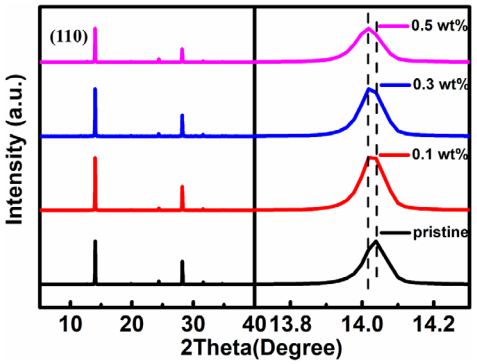

Figure 2. X-ray diffraction (XRD) of perovskite films with D-Asp-doped under different conditions.

(FWHM) compared with the pristine film, which indicates their larger grain size or better crystallinity. In addition, this diffraction peak shifted to low 2θ along with the increasing doping ratio of D-Asp, suggesting a slightly larger d-spacing and probable crystal structural distortion induced by D-Asp incorporation.[35]

We further characterized the film morphology using an atomic force microscope (AFM). Calculated from the height image (Figure S4a,b,d,e, Supporting Information), the roughness of the perovskite film decreased from 38.1 (pristine) to 30.5 nm (with 0.3 wt% of D-Asp). The smoother film morphology for the doped perovskite film should result in better contact and more uniform charge transport to the transporting layer. The phase image (Figure S4c,f, Supporting Information) again exhibits a larger grain size, which is consistent with previous characterizations.

To test the performance of D-Asp as an additive for PSCs, solar cell devices based on regular (n-i-p) architecture of ITO/SnO_2/perovskite (undoped or doped)/Spiro-OMeTAD/Au were fabricated as demonstrated by **Figure 3**a. The champion device was based on perovskite film doped with 0.3 wt% of D-Asp, which exhibited a remarkable PCE of 22.7%, a V_{OC} of 1.11 V, a FF of 81.0% and a J_{SC} of 25.25 mA cm^{-2}. This PCE is higher than that of all previously reported PSCs with natural amino acids as additives (Table S1, Supporting Information). Compared with the device based on pristine perovskite film with a PCE of 20.6%, the 10.2% enhancement of the PCE is also the highest among that of regular PSCs doped with natural amino acids (Table S1, Supporting Information). The PCE is almost stable within 300 s

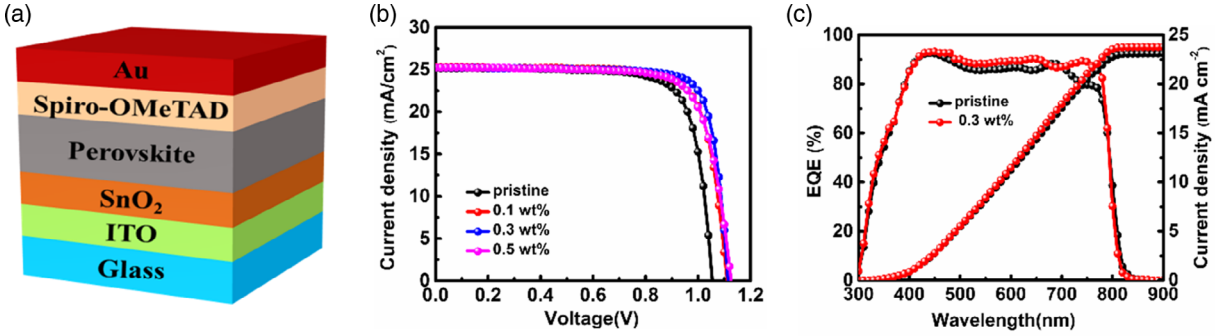

Figure 3. a) The device structure adopted in this study, b) *J–V* curves of the perovskite solar cells (PSCs) without or with different concentrations of D-Asp, and c) external quantum efficiency (EQE) of the PSCs without or with 0.3 wt% D-Asp.

using stabilized current at fixed voltage (SCFV) method,[36] validating the effectiveness of our measurement (Figure S5, Supporting Information). The *J*–*V* curves and the relevant device parameters are shown in Figure 3b and summarized in **Table 1**, respectively. In addition, as shown in Figure S6, Supporting Information, D-Asp doping could effectively narrow the statistical distribution of the FF, thus resulting in the narrowest PCE distribution of the device doped with 0.3 wt% of D-Asp, suggesting improved reproducibility.

We noticed that in the external quantum efficiency (EQE) curves (Figure 3c), devices with 0.3 wt% of D-Asp have a higher EQE response in a wide wavelength region than the device without D-Asp. The cross-sectional SEM images (**Figure 4**a,b) show different perovskite film thicknesses of 610 and 690 nm for undoped and doped ones, respectively. Adding D-Asp to the precursor solution should possibly change its viscosity, which results in a larger film thickness and higher absorption (Figure S7, Supporting Information). To eliminate the influence of the film thickness on the EQE response, we carefully dilute the precursor solution with 0.3 wt% of D-Asp and obtained a film thickness of 600 nm, which is close to the 610 nm of the pristine film (Figure S8, Supporting Information). From UV–vis absorption spectra, despite that the thinner doped perovskite film exhibited slightly decreased absorption than the pristine film (Figure S7, Supporting Information), the EQE of the corresponding device remain higher in a wide wavelength region (Figure S9, Supporting Information). Interestingly, under similar film thickness, the optical interference patterns of the pristine and doped films are distinct. This could possibly be due to the changed refractive index of the perovskite film upon doping. Therefore, we can conclude that the higher J_{SC} of the device doped with 0.3 wt% of D-Asp compared with the undoped device is the result of higher film thickness and improved charge transport and extraction processes. One important factor for charge transport and charge extraction efficiency is the morphology of the perovskite film. As a matter of fact, after doping 0.3 wt% of D-Asp, the bulk defects (such as cracks and pinholes) in the perovskite film are less obvious (Figure 4a,b), which is consistent with the morphologies of the neat films.

Table 1. The device parameters averaged from 20 devices with different doping ratio of asp.

Doping ratio [wt%]	V_{OC} [V]	J_{SC} [mA cm^{-2}]	FF [%]	PCE [%]	PCE_{max} [%]
0	1.04 ± 0.01	24.76 ± 0.31	74.3 ± 2.1	19.3 ± 0.7	20.6
0.1	1.09 ± 0.01	25.02 ± 0.62	75.3 ± 1.6	20.6 ± 0.6	21.7
0.3	1.09 ± 0.02	25.33 ± 0.27	77.3 ± 1.5	21.4 ± 0.6	22.7
0.5	1.10 ± 0.02	24.84 ± 0.42	75.2 ± 1.4	20.5 ± 0.6	21.7

The electronic behavior of the devices based on pristine and doped perovskites is also characterized by electrochemical impedance spectroscopy (EIS).[37,38] Figure 4c shows the equivalent circuit and Nyquist plots in the frequency range of 1 MHz–0.11 Hz under −0.3 V bias. It was observed that the Nyquist plots are semicircle and the recombination resistance (R_{rec}) increased from 2.7×10^4 (pristine) to $1.0 \times 10^5\ \Omega\,cm^2$ (with 0.3 wt% of D-Asp). The increase of R_{rec} is crucial in reducing the undesired charge recombination and improving V_{OC} of the device. The increased R_{rec} is also evidenced by the low leakage current of the device based on 0.3 wt% of D-Asp (Figure S10, Supporting Information). In contrast, upon doping of 0.3 wt% of D-Asp, the series resistance (R_S) of the device decreased from 26 to 14 $\Omega\,cm^2$, which means better device contacts and low parasitic resistance losses which may attribute to the better morphology of the doped perovskite film. Considering the aforementioned SEM results,[39,40] we conclude that D-Asp could greatly improve the morphology of the perovskite film thus resulting in improved device performance.

Another important factor affecting the charge transport and extraction efficiency is the defects in the perovskite film. To evaluate the defect passivation ability of D-Asp, we first characterized the hysteresis index (HI) of the devices through forward and reverse applied bias scanning (**Figure 5**a). It is well-known that the hysteresis in PSC is mainly affected by the ionic migration, polarization effects, and electronic charge trapping and de-trapping process, which are closely related to the defects in perovskite film.[41] The HI reduced from 17.7% to 12.9% when the pristine perovskite was doped with 0.3 wt% of D-Asp, which implies the effective suppression of defects by the additive.

The defect passivation effect of D-Asp was also evidenced by the photoluminescence (PL) behavior of the perovskite films. It was observed that the perovskite film doped with 0.3 wt% of D-Asp exhibited the highest PL intensity among all films (Figure 5b). The average PL decay lifetime is calculated to be 0.66 and 2.8 μs for the pristine perovskite film and film doped with 0.3 wt% of D-Asp, respectively (Figure 5c and Table S2, Supporting Information). The stronger PL emission and its longer lifetime of the doped film both suggest the suppression of the nonradiative processes, which are dominated by the defect-mediated Shockley–Read–Hall recombination.[42]

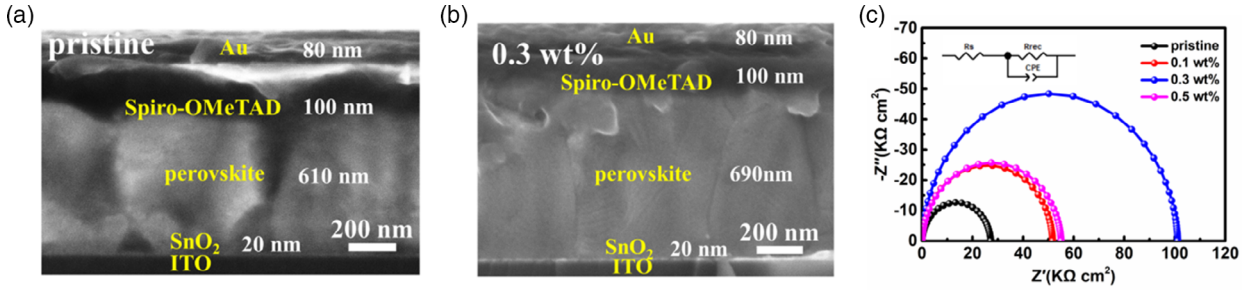

Figure 4. SEM image of the completed devices based on: a) pristine perovskite and b) perovskite doped with 0.3 wt% of D-Asp. c) Nyquist plot of PSCs without or with different concentrations of D-Asp. The inset shows the equivalent circuit.

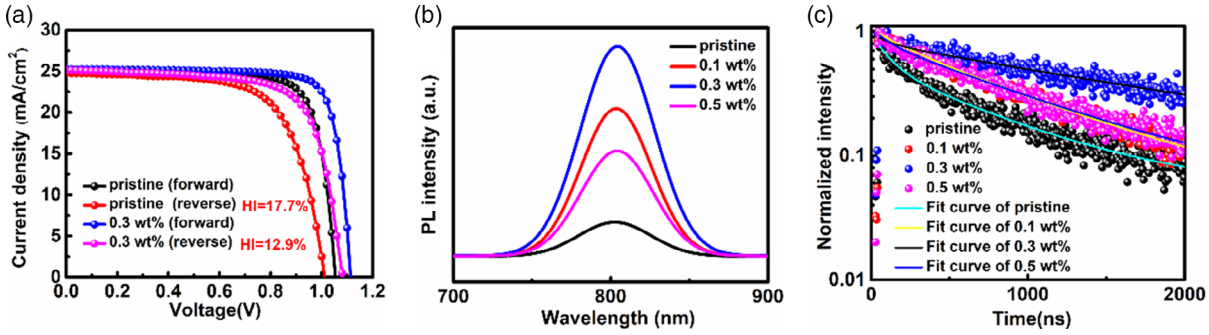

Figure 5. a) The best *J–V* data in forward and reverse scans, b) steady-state photoluminescence (PL) spectra of perovskite films with D-Asp-doped under different conditions, and c) time-resolved PL spectra of perovskite films with D-Asp-doped under different conditions.

The radiative and nonradiative recombination processes were further investigated by measuring the electroluminescence external quantum efficiency (EQE_{EL}) of the solar cell as a light-emitting diode (LED). As shown in **Figure 6**, the EQE_{EL} of the device based on 0.3 wt% of D-Asp reaches 5.04% at 25.25 mA cm^{-2} (J_{SC} under 1 sun) which outperforms the 0.45% EQE_{EL} (25.18 mA cm^{-2}) of the device based on pristine perovskite. The higher EQE_{EL} denotes more radiative behavior and reduced non-radiative loss. The open-circuit voltage loss (ΔV_{OC}) between doped and undoped devices was calculated by the following equation[43]

$$\Delta V_{OC} = \frac{k_B T}{q} \ln\left(\frac{EQE_{doped}}{EQE_{undoped}}\right) \quad (1)$$

In which k_B, T and q represent Boltzmann constant, temperature, and elementary charge, respectively. The ΔV_{OC} was calculated to be 0.063 V, which is in good agreement with the 0.06 V enhancement of the V_{OC} obtained from the *J–V* curves. Therefore, the high V_{OC} of the device doped with 0.3 wt% of D-Asp is mainly due to low defect-mediated non-recombination loss.

The detailed passivation mechanism of D-Asp was then studied using X-ray diffraction photoelectron spectroscopy (XPS) on the doped and undoped perovskite films. The whole XPS spectrum and individual spectra for Pb_{4f}, I_{3d}, N_{1s}, and O_{1s} are displayed in **Figure 7** and S11, Supporting Information,

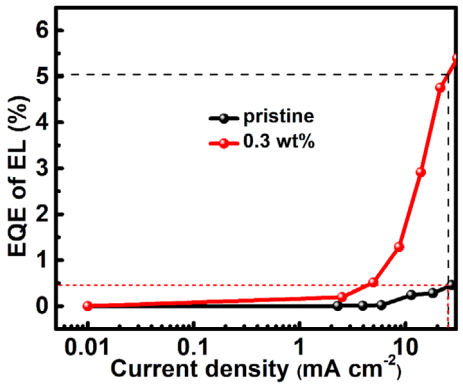

Figure 6. EQE of electroluminescence (EL) of the devices while operating as light-emitting diodes (LEDs).

respectively. It was found that the binding energy of Pb_{4f} increased and the binding energy of I_{3d} decreased when the pristine perovskite film was doped with 0.3 wt% of D-Asp, suggesting the change of electron density on these atoms. In contrast, the shift of the O_{1s} to higher binding energies suggests the interaction between –COOH/-COO^- and perovskite, probably in the form of coordination bonds occupying the X site vacancy.[44,45] Since the –NH_3...I—Pb hydrogen bonds occupying A site vacancy are widely observed for ammonium passivated perovskite, the electron density change on perovskite could be attributed to the hydrogen bond/coordination bond formation between perovskite and ammonium/carboxyl groups in D-Asp. Figure 7e,f exhibits the FTIR spectra of D-Aspartic acid and perovskite films without and with 0.3 wt% of D-Asp. The perovskite film with D-Asp has a stretching vibration at 3500–4000 cm^{-1} due to the formation of hydrogen bonds. The N–H (1610 cm^{-1}) stretching vibration of perovskite films with D-Asp is enhanced, indicating the formation of hydrogen bonds between amino and halogen atoms. As shown in Figure 7f, the -COO^- (1421 cm^{-1}) and C-O (1042 cm^{-1}) of D-Asp shifts to 1467 and 1048 cm^{-1} after the addition of D-Asp into the perovskite precursor solution, which is related to the coordination between carboxyl groups and Pb^{2+}. Based on the aforementioned analysis, the passivation mechanism of D-Asp involves passivation of A site and X site vacancy on the surface and grain boundaries of the perovskite film, which in turn improves the PCE and stability of the PSC devices. A schematic illustration of the perovskite film before and after D-Asp passivation is shown in Figure 7g.

The D-Asp additive not only improved the device performance of PSC devices, but also greatly enhanced their stability. As shown in **Figure 8**a, unencapsulated perovskite films with and without 0.3 wt% of D-Asp were stored in ambient condition with a relative humidity (RH) of 50% and a temperature of 30 °C. The pristine perovskite film mostly degraded after 96 h of storage, while the doped film was much less affected, demonstrating its excellent ambient stability. For the whole PSC devices, the PCE of the doped ones maintained 95% of the initial value after being stored in N_2 for 2000 h, which is better than the 93% of the undoped ones (Figure 8b). Even for the unencapsulated devices stored in ambient (20% RH at 30 °C), the PCE of the doped ones still could maintain 93% of the initial value after 3000 h, which is vastly improved from the 61% of the devices based on pristine perovskite (Figure 8c). To investigate the reason for the stability

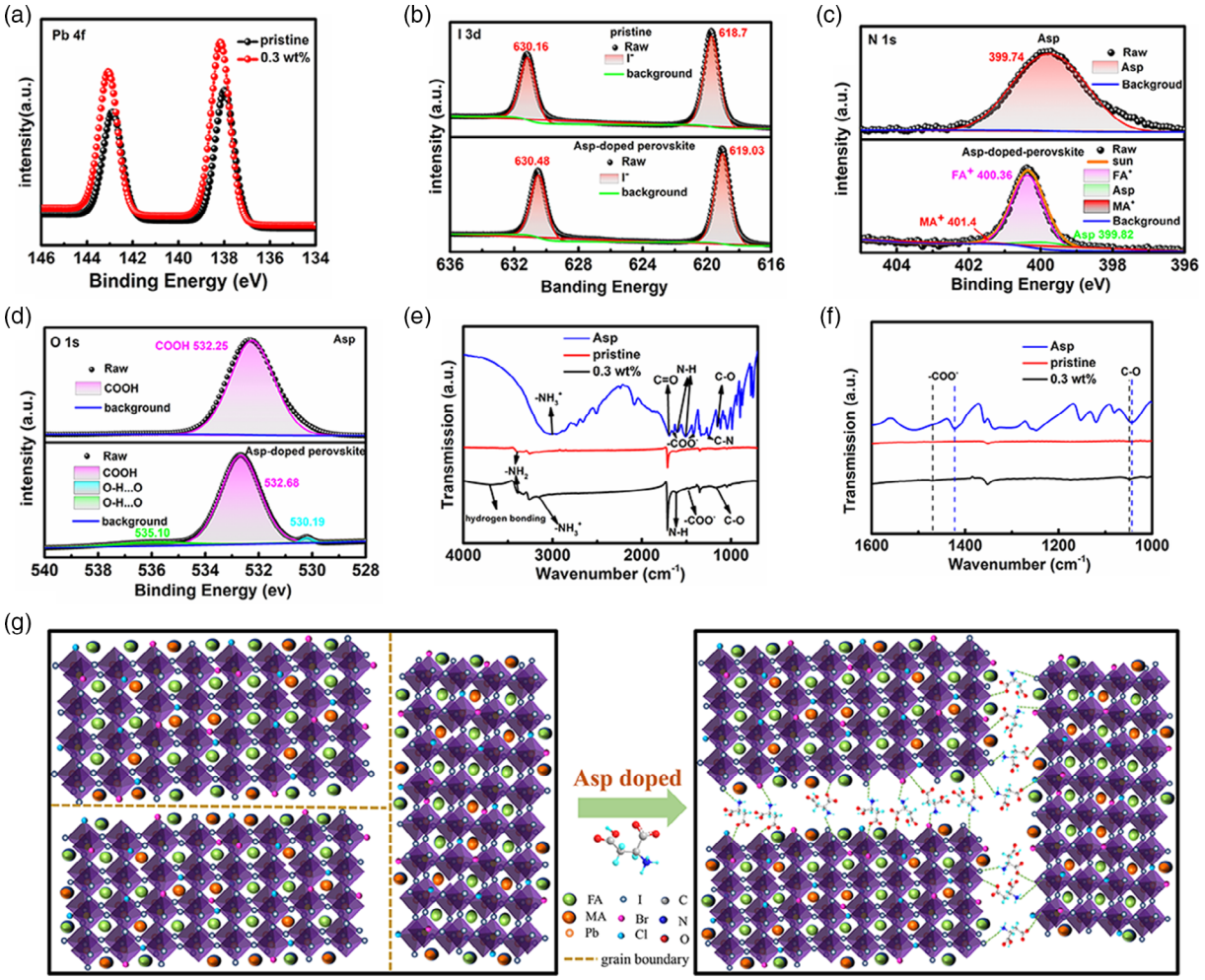

Figure 7. a) The Pb_{4f} X-ray diffraction photoelectron spectroscopy (XPS) spectra for pristine and 0.3 wt% D-Asp-doped perovskite films, b) the I_{3d} XPS spectra for pristine and 0.3 wt% D-Asp-doped perovskite films, c) the N_{1s} XPS spectra for D-Asp and 0.3 wt% D-Asp-doped perovskite films, d) the O_{1s} XPS spectra for D-Asp and 0.3 wt% D-Asp-doped perovskite films, e) Fourier transform infrared spectroscopy (FTIR) spectra of D-Asp and perovskite films without and with 0.3 wt% D-Asp, f) FTIR local enlarged view, and g) schematic diagram of perovskite crystals before (left) and after (right) passivation.

improvement, the contact angles between the doped/undoped perovskite films and water were measured, clearly showing a more hydrophobic surface of the doped ones (Figure S12, Supporting Information). Taking the previous results into account, the high stability of the PSC device based on perovskite doped with D-Asp could be attributed to the hydrophobicity of D-Asp on the surface, better morphology, and less defect-mediated degradation processes.

3. Conclusions

In summary, we applied a natural product, D-Aspartic acid, as an additive in mixed ion perovskite solar cells with regular architecture. The thickness of the perovskite film increased upon doping which enabled higher light absorption and the morphology of the perovskite film was improved with fewer cracks and pinholes. The amino and carboxyl groups in D-Asp simultaneously passivated the A site vacancy and uncoordinated Pb^{2+} sites, which in turn reduced the defect density of perovskite significantly. The champion PCE of the device doped with D-Asp reached 22.7%, which is higher than that of all previously reported PSCs doped with natural amino acids. In addition, the great device stability was evidenced by the 93% of the initial PCE for the unencapsulated PSCs stored in ambient with RH of 20% and temperature of 30 °C. This work suggests that D-Asp, as a multifunctional natural product, could be a good additive candidate for state-of-the-art mixed ion PSCs with regular architecture. And organic additives with multiple functional groups could greatly enhance the performance of PSCs even with a small doping ratio, which could simplify the fabrication process and reduce the overall cost of the devices.

4. Experimental Section

Materials: N,N-dimethylformamide (DMF), dimethyl sulfoxide (DMSO), and chlorobenzene (CB) were purchased from Aladdin. Lead iodide beads (PbI_2) and tin oxide (SnO_2) colloid solution were obtained from Alfa Aesar.

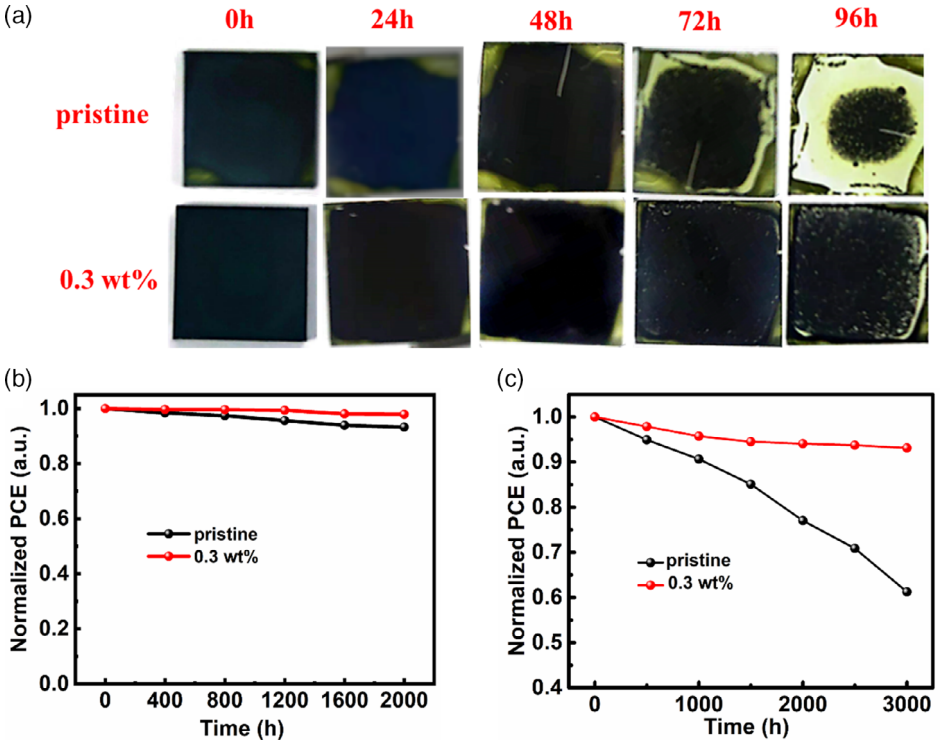

Figure 8. a) Images of perovskite films under 50% RH and 30 °C, b) the stability of the PSCs under N_2, and c) the stability of the PSCs under 20% RH and 30 °C.

D-Aspartic acid was purchased from Aladdin. Formamidinium iodide (FAI) was purchased from Great Cell Solar (Australia). Spiro-OMeTAD was purchased from Lumtec. Methylammonium bromide (MABr), methylammonium chloride (MACl), lead bromide ($PbBr_2$) lithium bis (trifluoromethylsulfonyl) imide (Li-TFSI) were bought from Xi'an Polymer Light Technology Corp. All chemicals were used as received without further purification.

Device Fabrication: First, indium-doped tin oxide (ITO) glasses were washed and sonicated in detergent, deionized (DI) water, and isopropanol (IPA) for 20 min each, and dried under a nitrogen gun. Then, the substrates were subjected to ultraviolet-ozone treatment for 20 min. The thin film of SnO_2 (2.5%) was deposited by spin-coating onto the ITO substrate at 3000 rpm for 30 s. and then annealed at 150 °C for 30 min in ambient condition. Then perovskite precursor solution was prepared by mixing 696 mg (1.5 M) of PbI_2, 240.76 mg (1.4 M) of FAI, 11 mg (0.03 M) of $PbBr_2$, 3.36 mg (0.03 M) of MABr, 33.75 mg (0.5 M) of MACl, 0.1–3 wt% of aspartic acid (0.98, 2.95, 4.9, 9.8, 29.5 mg) in a mixture solvent (DMF:DMSO = 4:1). A one-step method was used to prepare perovskite films. The perovskite precursor solution was spin-coated at 5000 rpm for 30 s, then 150 µL CB was dropped onto the spinning substrate after 25 s, followed by annealing at 150 °C for 40 min. The Spiro-OMeTAD solution was spin-coated on the perovskite layer at 4000 rpm for 30 s. The Spiro-OMeTAD solution was prepared by mixing 72.3 mg Spiro-OMeTAD, 35 µL bis(trifluoromethane) sulfonamide lithium salt (Li-TFSI) stock solution (260 mg Li-TFSI in 1 mL acetonitrile), 30 µL 4-tertbutylpyridine(TBP), and 1 mL chlorobenzene(CB). Finally, Au (80 nm) was thermally evaporated under a pressure of 1.4×10^{-4} Pa. The device area is 0.04 cm^2.

Characterizations: The UV–vis absorption spectra were measured using a U-3501 spectrophotometer (Hitachi). The XRD patterns were carried out using a D8 ADVANCE XRD equipment. The current density–voltage (*J–V*) curves were characterized by a Keithley 2400 source meter unit under one-sun AM 1.5G illumination (100 mW cm^{-2}) with a solar light simulator (SS-F5-3A, Enlitech, Taiwan) The devices are tested without pretest illumination and bias poling, and the scan rate was 0.2 V s^{-1}. The EQE spectra are obtained using a QE-R 3011 system (Enlitech, Taiwan) in the range of 300–900 nm. The stabilized current at fixed voltage (SCFV) method was applied following established protocols.[36] The voltage was set to 0.88 (pristine) and 0.94 V (with 0.3 wt% of D-Asp) at the maximum power point to measure current and efficiency continuously. PL measurements of perovskite films on glass were conducted using an Edinburgh FLSP920 spectrophotometer installed with an excitation source of 440 nm picosecond pulsed diode laser with an average power of 0.15 mW. The XPS spectra of perovskite films on ITO glass substrates were carried out by using Thermo Scientific K-Alpha+. The SEM images were obtained using a Hitachi S-4800 field emission scanning electron microscopy. Nano Measurer software was used to determine the grain sizes in the SEM images.

Supporting Information

Supporting Information is available from the Wiley Online Library or from the author.

Acknowledgements

The authors thank the National Natural Science Foundation of China (22005202) and the Scientific Research Startup Fund for Shenzhen High-Caliber Personnel of SZPT (6022310054k) for financial Support.

Conflict of Interest

The authors declare no conflict of interest.

Data Availability Statement

The data that support the findings of this study are available from the corresponding author upon reasonable request.

Keywords

additives, aspartic acid, defect passivation, morphology control, perovskite solar cells

Received: November 3, 2022
Revised: November 28, 2022
Published online: December 18, 2022

[1] K. Dong, Y. Han, Y. Dou, M. Shahbaz, *Sustainable Dev.* **2021**, *30*, 751.
[2] A. Kojima, K. Teshima, Y. Shirai, T. Miyasaka, *J. Am. Chem. Soc.* **2009**, *131*, 6050.
[3] National Renewable Energy Laboratory Best Research-Cell Efficiency Chart, https://www.nrel.gov/pv/cell-efficiency.html (accessed: May 2022).
[4] W. Shockley, H. J. Queisser, *J. Appl. Phys.* **1961**, *32*, 510.
[5] B. T. van Gorkom, T. P. A. van der Pol, K. Datta, M. M. Wienk, R. A. J. Janssen, *Nat. Commun.* **2022**, *13*, 349.
[6] Y. Zhao, T. Heumueller, J. Zhang, J. Luo, O. Kasian, S. Langner, C. Kupfer, B. Liu, Y. Zhong, J. Elia, A. Osvet, J. Wu, C. Liu, Z. Wan, C. Jia, N. Li, J. Hauch, C. J. Brabec, *Nat. Energy* **2022**, *7*, 144.
[7] Y. Jiang, L. Qiu, E. J. Juarez-Perez, L. K. Ono, Z. Hu, Z. Liu, Z. Wu, L. Meng, Q. Wang, Y. Qi, *Nat. Energy* **2019**, *4*, 585.
[8] R. Wang, M. Mujahid, Y. Duan, Z. K. Wang, J. Xue, Y. Yang, *Adv. Funct. Mater.* **2019**, *29*, 1808843.
[9] E. Bi, H. Chen, F. Xie, Y. Wu, W. Chen, Y. Su, A. Islam, M. Gratzel, X. Yang, L. Han, *Nat. Commun.* **2017**, *8*, 15330.
[10] H. Min, D. Y. Lee, J. Kim, G. Kim, K. S. Lee, J. Kim, M. J. Paik, Y. K. Kim, K. S. Kim, M. G. Kim, T. J. Shin, S. Il Seok, *Nature* **2021**, *598*, 444.
[11] D. Yang, R. Yang, K. Wang, C. Wu, X. Zhu, J. Feng, X. Ren, G. Fang, S. Priya, S. Liu, *Nat. Commun.* **2018**, *9*, 3239.
[12] W. Ke, C. C. Stoumpos, J. L. Logsdon, M. R. Wasielewski, Y. Yan, G. Fang, M. G. Kanatzidis, *J. Am. Chem. Soc.* **2016**, *138*, 14998.
[13] Q. Jiang, Y. Zhao, X. Zhang, X. Yang, Y. Chen, Z. Chu, Q. Ye, X. Li, Z. Yin, J. You, *Nat. Photonics* **2019**, *13*, 460.
[14] F. Ali, C. Roldán-Carmona, M. Sohail, M. K. Nazeeruddin, *Adv. Energy Mater.* **2020**, *10*, 2002989.
[15] Y. Li, Y. Zhao, Q. Chen, Y. M. Yang, Y. Liu, Z. Hong, Z. Liu, Y. T. Hsieh, L. Meng, Y. Li, Y. Yang, *J. Am. Chem. Soc.* **2015**, *137*, 15540.
[16] A. Agresti, A. Pazniak, S. Pescetelli, A. Di Vito, D. Rossi, A. Pecchia, M. Auf der Maur, A. Liedl, R. Larciprete, D. V. Kuznetsov, D. Saranin, A. Di Carlo, *Nat. Mater.* **2019**, *18*, 1228.
[17] X. Yao, L. Zheng, X. Zhang, W. Xu, W. Hu, X. Gong, *ACS Appl. Mater. Interfaces* **2019**, *11*, 40163.
[18] Z. Ma, W. Zhou, D. Huang, Q. Liu, Z. Xiao, H. Jiang, Z. Yang, W. Zhang, Y. Huang, *ACS Appl. Mater. Interfaces* **2020**, *12*, 52500.
[19] F. Zhang, K. Zhu, *Adv. Energy Mater.* **2019**, *10*, 1902579.
[20] S. Wafee, B. H. Liu, C.-C. Leu, *Mater. Today Energy* **2021**, *22*, 100847.
[21] W. Feng, C. Zhang, J. X. Zhong, L. Ding, W. Q. Wu, *Chem. Commun.* **2020**, *56*, 5006.
[22] W.-Q. Wu, Z. Yang, P. N. Rudd, Y. Shao, X. Dai, H. Wei, J. Zhao, Y. Fang, Q. Wang, Y. Liu, Y. Deng, X. Xiao, Y. Feng, J. Huang, *Sci. Adv.* **2019**, *5*, eaav8925.
[23] T. Wu, Y. Wang, X. Li, Y. Wu, X. Meng, D. Cui, X. Yang, L. Han, *Adv. Energy Mater.* **2019**, *9*, 1803766.
[24] X. Li, C.-C. Chen, M. Cai, X. Hua, F. Xie, X. Liu, J. Hua, Y.-T. Long, H. Tian, L. Han, *Adv. Energy Mater.* **2018**, *8*, 1800715.
[25] S.-C. Yun, S. Ma, H.-C. Kwon, K. Kim, G. Jang, H. Yang, J. Moon, *Nano Energy* **2019**, *59*, 481.
[26] C. T. Lin, W. Xu, T. J. Macdonald, J. Ngiam, J. H. Kim, T. Du, S. Xu, P. S. Tuladhar, H. Kang, K. Lee, J. R. Durrant, M. A. McLachlan, *ACS Appl. Mater. Interfaces* **2021**, *13*, 43505.
[27] J. H. Kim, Y. R. Kim, B. Park, S. Hong, I. W. Hwang, J. Kim, S. Kwon, G. Kim, H. Kim, K. Lee, *Small* **2021**, *17*, e2005608.
[28] J. Hu, X. Xu, Y. Chen, S. Wu, Z. Wang, Y. Wang, X. Jiang, B. Cai, T. Shi, C. J. Brabec, Y. Mai, F. Guo, *J. Mater. Chem. A* **2021**, *9*, 5857.
[29] A. Karavioti, E. Vitoratos, E. Stathatos, *J. Mater. Sci.: Mater. Electron.* **2020**, *31*, 6109.
[30] H. Yuan, Z. Zhang, T. Guo, L. Yu, Z. Deng, R. Zhao, J. Zhang, Y. Zhu, *J. Alloy. Compd.* **2021**, *876*, 160140.
[31] W. Zhang, X. Lei, J. Liu, J. Dong, X. Yan, W. Gao, H. Dong, C. Ran, Z. Wu, *Phys. Status Solidi RRL* **2019**, *13*, 1800505.
[32] J. J. Yoo, G. Seo, M. R. Chua, T. G. Park, Y. Lu, F. Rotermund, Y. K. Kim, C. S. Moon, N. J. Jeon, J. P. Correa-Baena, V. Bulovic, S. S. Shin, M. G. Bawendi, J. Seo, *Nature* **2021**, *590*, 587.
[33] T. H. Han, J. W. Lee, C. Choi, S. Tan, C. Lee, Y. Zhao, Z. Dai, N. De Marco, S. J. Lee, S. H. Bae, Y. Yuan, H. M. Lee, Y. Huang, Y. Yang, *Nat. Commun.* **2019**, *10*, 520.
[34] A. Bonadio, C. A. Escanhoela, F. P. Sabino, G. Sombrio, V. G. de Paula, F. F. Ferreira, A. Janotti, G. M. Dalpian, J. A. Souza, *J. Mater. Chem. A* **2021**, *9*, 1089.
[35] Y. Ren, N. Zhang, Z. Arain, M. Mateen, J. Chen, Y. Sun, Z. Li, *J. Power Sources* **2020**, *475*, 228676.
[36] R. B. Dunbar, B. C. Duck, T. Moriarty, K. F. Anderson, Noel W. Duffy, C. J. Fell, J. Kim, A. Ho-Baillie, D. Vak, T. Duong, Y. Wu, K. Weber, A. Pascoe, Y.-B. Cheng, Q. Lin, P. L. Burn, R. Bhattacharjee, H. Wang, G. J. Wilson, *J. Mater. Chem. A* **2017**, *5*, 22542.
[37] A. Guerrero, J. Bisquert, G. Garcia-Belmonte, *Chem. Rev.* **2021**, *121*, 14430.
[38] E. von Hauff, D. Klotz, *J. Mater. Chem. C* **2022**, *10*, 742.
[39] L. Contreras-Bernal, S. Ramos-Terrón, A. Riquelme, P. P. Boix, J. Idígoras, I. Mora-Seró, J. A. Anta, *J. Mater. Chem. A* **2019**, *7*, 12191.
[40] T. S. Sherkar, C. Momblona, L. Gil-Escrig, J. Avila, M. Sessolo, H. J. Bolink, L. J. A. Koster, *ACS Energy Lett.* **2017**, *2*, 1214.
[41] D. H. Kang, N. G. Park, *Adv. Mater.* **2019**, *31*, e1805214.
[42] A. Solanki, M. M. Tavakoli, Q. Xu, S. S. H. Dintakurti, S. S. Lim, A. Bagui, J. V. Hanna, J. Kong, T. C. Sum, *Adv. Mater.* **2020**, *32*, e1907864.
[43] W. Tress, N. Marinova, O. Inganäs, M. K. Nazeeruddin, S. M. Zakeeruddin, M. Graetzel, *Adv. Energy Mater.* **2015**, *5*, 1400812.
[44] T. Zheng, L. Fan, H. Zhou, Y. Zhao, B. Jin, R. Peng, *ACS Appl. Mater. Interfaces* **2020**, *12*, 24747.
[45] Z. Fang, W. Chen, Y. Shi, J. Zhao, S. Chu, J. Zhang, Z. Xiao, *Adv. Funct. Mater.* **2020**, *30*, 1909754.